

# Strategy for Multi-Scale Single-Phase Flow Coupling

---

Nuclear Engineering Division

**About Argonne National Laboratory**

Argonne is a U.S. Department of Energy laboratory managed by UChicago Argonne, LLC under contract DE-AC02-06CH11357. The Laboratory's main facility is outside Chicago, at 9700 South Cass Avenue, Argonne, Illinois 60439. For information about Argonne and its pioneering science and technology programs, see [www.anl.gov](http://www.anl.gov).

**Availability of This Report**

This report is available, at no cost, at <http://www.osti.gov/bridge>. It is also available on paper to the U.S. Department of Energy and its contractors, for a processing fee, from:

U.S. Department of Energy  
Office of Scientific and Technical Information  
P.O. Box 62  
Oak Ridge, TN 37831-0062  
phone (865) 576-8401  
fax (865) 576-5728  
[reports@adonis.osti.gov](mailto:reports@adonis.osti.gov)

**Disclaimer**

This report was prepared as an account of work sponsored by an agency of the United States Government. Neither the United States Government nor any agency thereof, nor UChicago Argonne, LLC, nor any of their employees or officers, makes any warranty, express or implied, or assumes any legal liability or responsibility for the accuracy, completeness, or usefulness of any information, apparatus, product, or process disclosed, or represents that its use would not infringe privately owned rights. Reference herein to any specific commercial product, process, or service by trade name, trademark, manufacturer, or otherwise, does not necessarily constitute or imply its endorsement, recommendation, or favoring by the United States Government or any agency thereof. The views and opinions of document authors expressed herein do not necessarily state or reflect those of the United States Government or any agency thereof, Argonne National Laboratory, or UChicago Argonne, LLC.

# Strategy for Multi-Scale Single-Phase Flow Coupling

---

prepared by  
R. Hu, J. W. Thomas, and T. H. Fanning  
Nuclear Engineering Division, Argonne National Laboratory

March 31, 2013



## EXECUTIVE SUMMARY

For practical nuclear engineering applications, multi-scale analysis by adopting the combined use of different scale computational tools, such as system thermal-hydraulics and CFD codes is vital when three-dimensional effects play an important role in the evolution of a given transient or accident scenario. The feasibility of coupling low-fidelity systems codes with higher fidelity CFD tools was demonstrated previously under NEAMS by coupling SAS4A/SASSYS-1 with the commercial CFD code STAR-CD and STAR-CCM+. An “ad-hoc” coupling strategy was implemented. With the advances in numerical techniques and software engineering, such as the availability of PETSc and MOOSE, modernization of existing systems codes or the development of new system code becomes more compelling. MOOSE (Multi-physics Object Oriented Simulation Environment) is a parallel computational framework developed at INL for enabling the solution of complex, fully-implicit multi-physics systems. It has been utilized in many nuclear applications including the system analysis codes RELAP-7 and the SFR module under current NEAMS Reactor Product Line (RPL). This motivates the development of a coupled scheme for MOOSE-based system analysis code and the commercial CFD code STAR-CCM+. STAR-CCM+ is a general-purpose commercial CFD code using finite volume formulation for the analysis of compressible and incompressible flows and heat transfer, and it is being included in the toolkit of the NEAMS RPL. This investigation is important for the integration between the MOOSE-based system codes and the high-fidelity advanced simulation capabilities developed under the NEAMS RPL.

Careful control of data exchange flow and the time-synchronization is essential for a numerically stable, and physically valid coupled code simulation. The general issues of coupling of system code and CFD code have been addressed in this report, including data exchange method, driving mechanism, time synchronization scheme, and the selection of data for exchange. Then the coupling strategy between the MOOSE-based system analysis code for SFR and CFD code STAR-CCM+ was derived and implemented based on these considerations and the characteristics of each code. The developed strategy for the coupling of MOOSE-based system codes and STAR-CCM+ is applicable to other multi-scale or multi-physics code coupling applications.

A simple test model was developed to examine the coupling strategy and its implementation in the system code and CFD code. The flow loop of the test model consists of one tank, one pump, and four pipes. In the coupled simulation, the tank, with cover gas, was modeled by STAR-CCM+, while the rest of the hydraulic loop was modeled by the system code. The coupling strategy was demonstrated by the three test cases: steady state, flow transient, and temperature transient. Stand-alone system code simulations have also been performed to examine the differences and consistency between the couple code and stand-alone system code simulations.

In steady-state simulations, the pressure difference between the tank inlet and tank outlet is 5.1 kPa in the stand-alone system code simulation, while it is 5.2 kPa in the coupled simulation. This small difference is because the friction pressure loss in the tank is ignored in the stand-alone system model, and the form loss coefficients are assumed zeros in the test problem. The differences in the pressure drop caused slightly different (0.24%) velocity

predictions in the two simulations. The steady-state differences in the two simulations can be easily removed by providing adjusted form loss coefficients in the stand-alone system code model. The differences between the coupled code and stand-alone system code simulations are very small during the whole flow (pump head reduction) transient, only slightly higher than the difference in the steady-state results. This is expected since a 0-D or 3-D representation of the tank has negligible effects to pressure wave propagation.

The temperature transient was developed to examine the effects of thermal stratification in a large tank and to demonstrate the significance of the coupled multi-scale simulation. Strong thermal stratification in the tank has been observed in the coupled simulation during the entire transient. The tank inlet temperature responses were almost the same for the first 35 seconds of the transient in both the coupled code and stand-alone system code simulations. But the tank outlet temperature responses from the two simulations were very different due to the thermal stratification in the tank. In the coupled code simulation, the tank outlet temperature remained unchanged for more than 20 seconds, and then decreased very slowly during the entire transient. In the stand-alone system code simulation, the tank inlet temperature quickly increased after the cooling transient, exceeded the tank outlet temperature, and then dropped below the tank outlet temperature. This pattern repeated as the solution approaches a new steady state. This behavior was not observed in this in the coupled code simulation.

These preliminary results provided a proof-of-principle of coupling the two codes, and have demonstrated the significance of the coupled code for applications that three-dimensional effects play an important role in the evolution of a given accident scenario. Future investigations would include the continuous testing, verification, and validation of the coupled code, and the applications to the safety simulations of the advanced liquid-metal reactor designs, in addition to the continuous development of physics modeling and component designs for the MOOSE-based SFR system analysis module.

## TABLE OF CONTENTS

Executive Summary.....	i
Table of Contents .....	iii
List of Figures.....	v
List of Tables.....	vi
1 Introduction.....	1
2 General Considerations.....	1
2.1 Data Exchange Method .....	2
2.2 Driving Mechanism for Coupled Code Execution.....	2
2.3 Time Synchronization Scheme.....	3
2.4 Selection of the Boundary Conditions at the Coupling Interface.....	4
3 Coupling Strategy between MOOSE-Based System Codes and STAR-CCM+.....	6
4 Implementation of the Coupling Strategy.....	8
4.1 Implementation in the System Code.....	8
4.2 Implementation in STAR-CCM+.....	9
5 Demonstration of the Coupling Strategy .....	10
5.1 Description of the Test Problems .....	10
5.1.1 System Model of the Loop.....	10
5.1.2 CFD Model of the Tank.....	11
5.2 Steady-State Simulation Results.....	14
5.3 Flow Transient Simulations.....	17
5.4 Temperature Transient Simulations .....	20
5.4.1 Cooling Transient Results.....	20
5.4.2 Non-Isothermal Flow Approaching Steady-State.....	22
6 Summary and Future Work.....	27
References .....	29





## LIST OF FIGURES

Figure 1: Multiple Codes Coupling Scheme .....	3
Figure 2: Coupling Schemes for a Generic Time Step.....	4
Figure 3: Data Flow for Boundary Coupling .....	5
Figure 4: Domain Overlapping Coupling Scheme .....	6
Figure 5: Data Exchange Scheme for the Coupling between the MOOSE-based System Codes and the CFD Code STAR-CCM+ .....	7
Figure 6: Execution Process Flow Chart of the CoupledCFDExecutioner .....	8
Figure 7: Sample Input Block for the CoupledCFDExecutioner .....	9
Figure 8: Schematics of the Test Problem.....	10
Figure 9: The Loop Model in the System Code .....	11
Figure 10: Side View of the STAR-CCM+ Geometry for the Test Problem.....	13
Figure 11: CFD Mesh on the Vertical Plane Slicing through the Centers of the Inlet and Outlet Boundary Surfaces: Entire Plane (left) and Vicinity of the Inlet Junction (right).....	14
Figure 12: CFD Prediction for the Velocity Field at the Initial Condition at the Vertical Plane Slicing through the Centers of the Inlet and Outlet Boundary Surfaces .....	15
Figure 13: CFD Prediction for the Sodium Volume Fraction at the Initial Condition at the Vertical Plane Slicing through the Centers of the Inlet and Outlet Boundary Surfaces.....	15
Figure 14: CFD Prediction for the Pressure at the Initial Condition at the Vertical Plane Slicing through the Centers of the Inlet and Outlet Boundary Surfaces .....	16
Figure 15: Pressure Distributions in the loop of the Stand-alone Steady-State Simulation.....	17
Figure 16: Pre-defined Pump Head during the Flow Transient .....	17
Figure 17: CFD Prediction for the Velocity Profile Evolution during the Flow Transient.....	19
Figure 18: Comparison of Mass Flow Rates at Tank Inlet during the Flow Transient .....	20
Figure 19: CFD Prediction for the Temperature Evolution during the Cooling Transient .....	21
Figure 20: Comparison of Tank Inlet and Outlet Temperature during the Cooling Transient.....	22
Figure 21: CFD Prediction for the Temperature Evolution after Cooling Transient .....	24
Figure 22: Comparison of Tank Inlet and Outlet Temperature during the Temperature Transient after Cooling, $T = 0 - 30$ s .....	25
Figure 23: Comparison of Tank Inlet and Outlet Temperature during the Temperature Transient after Cooling, $T = 30 - 300$ s .....	25
Figure 24: Temperature Distribution of the Loop System, $T = 2$ s.....	26
Figure 25: Temperature Distribution of the Loop System, $T = 20, 40, \text{ or } 300$ s .....	26
Figure 26: CFD Prediction of the Temperature Distribution in the Tank, $T = 300$ s .....	27

## LIST OF TABLES

Table 1: Component Parameters of the Test Loop Model in System Code.....	11
Table 2: Geometry of the Test Tank Model in STAR-CCM+ .....	13

## 1 Introduction

Recent advances in computational fluid dynamics (CFD) codes along with high performance computing hardware make the codes more useful in many engineering applications. For instance, single-phase CFD codes have been used to predict fluid flow in fuel channels of both pressurized water reactors (PWR) [1] and sodium fast reactors (SFR) [2]. However, a whole core simulation with explicit representation of wire wraps and spacer grids would require tens of billions of computational cells and remains impractical for the near term. Certainly, transient CFD analysis of the response of the entire reactor primary coolant system and core to an off-normal or design-basis event would be difficult to achieve even with high-performance computers. For more practical engineering applications, the concept of “multi-scale” analysis has been proposed [3,4] by adopting the combined use of different scale computational tools, such as system thermal-hydraulics and CFD codes. This coupling between system and CFD codes is vital when three-dimensional effects play an important role in the evolution of a given accident scenario.

Previously under NEAMS, the feasibility of coupling low-fidelity systems codes with higher fidelity CFD tools was demonstrated by coupling the legacy system code SAS4A/SASSYS-1 [5] with the commercial CFD code STAR-CD [6]. The importance of developing a multi-resolution capability was demonstrated by evaluating the formation of thermal stratification layers in the outlet plenum of a sodium-cooled fast reactor (SFR) during a postulated loss-of-flow accident. An “ad-hoc” coupling strategy was implemented, partially due to the limitations in the code structure of SAS4A/SASSYS-1. With the advances in numerical techniques and software engineering, such as the availability of PETSc [7] and MOOSE [8], modernization of existing systems codes or the development of new system code becomes more compelling. MOOSE (Multi-physics Object Oriented Simulation Environment) is a parallel computational framework developed at INL for enabling the solution of complex, fully-implicit multi-physics systems. It has been utilized in many nuclear applications including the system analysis codes RELAP-7 [9] along with the SFR module [10] under the current NEAMS Reactor Product Line (RPL). This motivates the development of a coupled scheme for MOOSE-based system analysis codes and the commercial CFD code STAR-CCM+ [11]. STAR-CCM+ is a general-purpose commercial CFD code that uses a finite volume formulation for the analysis of compressible and incompressible flows and heat transfer. It has been applied to a wide variety of nuclear reactor analyses in the national laboratories, academia, and industry.

This report begins with a general discussion of the general issues of code-to-code coupling, which may be applicable to both multi-physics coupling and multi-scale coupling. This is followed by a description of the implementation of the coupling scheme in the MOOSE-based SFR system analysis module and STAR-CCM+ for multi-scale safety analysis of SFR transients. Preliminary results of the coupled code are presented for several test problems, followed by discussion of future work and concluding remarks.

## 2 General Considerations

Many applications of coupling system codes with CFD codes can be found in the literature, such the above-mentioned coupling between SAS4A/SASSYS-1 and STAR-CD

[5]. Fanning and Thomas also extended the coupling to SAS4A/SASSYS-1 and STAR-CCM+ [12]. Aumiller et al. presented a coupling between the system code RELAP5 and an early version of CFX [13]. Bertolotto et al. coupled TRACE and CFX codes and demonstrated the advantages of a 3D simulation over a 1D approximation [14]. In all applications, careful control of data exchange flow and the time-synchronization are essential for a numerically stable, and physically valid simulation. Very different coupling schemes were used, partially due to the different features and limits within the specific codes. In this section, various issues in the coupling between a system code and a CFD code are discussed, including data exchange method, driving mechanism, time synchronization scheme, and the selection of data for exchange.

### **2.1 Data Exchange Method**

The basic requirement of multi-code coupling is that information can be exchanged among them. The data being exchanged depends on other coupling strategies, such as one-way or two-way coupling, loose or tight coupling, driving mechanism, and time synchronization, etc. Many options are available and often open source, including file I/O (read/write data exchange files), sockets, database, message passing, etc. The choice would be dependent on the amount of exchanged data, the number of parallel computing processors, and the data synchronization scheme. As will be discussed in the following section, the MOOSE-based SFR code and STAR-CCM+ codes are initially utilizing simple file I/O, but more sophisticated options will be considered for future work.

### **2.2 Driving Mechanism for Coupled Code Execution**

Two different driving schemes for coupled code execution are shown in Figure 1. In the Master-Slave scheme, one code, usually the system code, is defined as the “master” and bears the task of directing the information exchange with the other codes, i.e. the “slaves”. In the other approach, an external executable is developed solely to manage the data exchange and to drive the calculation process of the coupled code system. The selection of the driving mechanism is generally a developer’s preference. However, an external driver could be more modular, thus preferable, in multi-code coupling on high-performance computers. The choice of driving mechanism needs to be made alongside the choice of the time synchronization scheme, as will be discussed next. The master-slave scheme in Figure 1a was selected for the coupling between the MOOSE-based SFR code and STAR-CCM+.

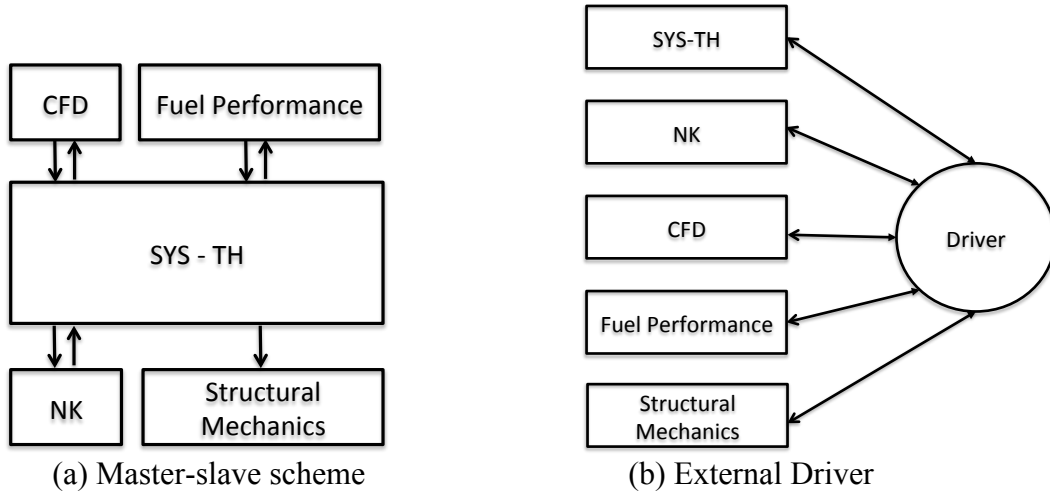
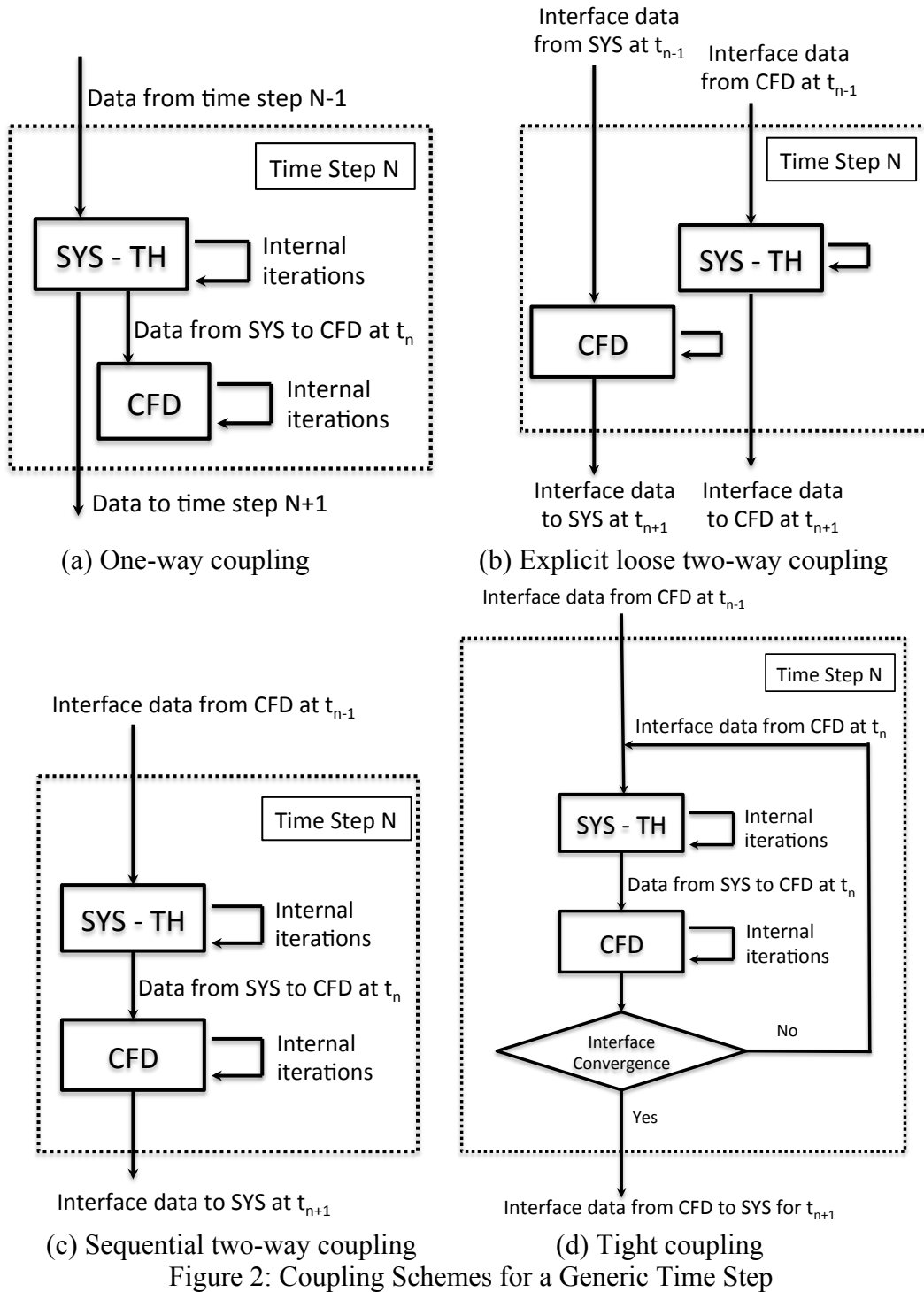


Figure 1: Multiple Codes Coupling Scheme

### 2.3 Time Synchronization Scheme

The synchronization of data exchange is crucial to the accuracy and the convergence of the coupled code system. Four different coupling schemes are listed in Figure 2 for multi-scale coupling between a system thermal-hydraulics code (SYS-TH) and a CFD code. In all four schemes, the SYS-TH code is chosen as the master to drive the data exchange and coupled code execution. This is a practical choice, given that the majority of the problem domain is being modeled with the SYS-TH code, and SYS-TH codes often manage transient responses to a wide range of physics conditions (e.g. thermal-hydraulics, neutron kinetics, fuel behavior, structural mechanics) even when not coupled to external codes. Note that the meaning of the terminologies in this report could be different among different group of researchers, regarding to loose (weak) vs. tight (strong), explicit vs. implicit.

In Figure 2a, a one-way or explicit loose (weak) coupling method is used. In this approach, the simulation results obtained from SYS-TH code (coarse mesh) are transferred to the CFD code as boundary conditions for a refined calculation with a finer scale mesh. The simulation results of the CFD code are not sent back, thus do not affect the simulation of the SYS-TH code. In the explicit loose two-way coupling scheme (Figure 2b), the results of both codes are exchanged at the coupling interface. However, at each time step, the boundary conditions of both codes are using the information calculated by the other code at the previous time step. In Figure 2c, some implicitness is added in the sequential two-way coupling scheme. Although the SYS-TH code is using the information from the CFD code results at the previous time step, the CFD code uses the concurrent information from SYS-TH code at the same time step. In both two-way coupling methods depicted in Figure 2b and Figure 2c, special care needs to be taken for the numerical stability of the coupled code. To make sure the results are consistent at the boundary interface between the two codes, an interface consistence check is added in the tight two-way coupling scheme, shown in Figure 2d. In this scheme, the same time step is repeated in both SYS-TH and CFD until the convergence at the interface between the two codes is reached. This approach is the strongest coupling scheme a developer can get without going deep in modifying the source codes of the CFD and SYS-TH codes. However, this approach can be expensive since it requires multiple CFD calculations within a time-step.



#### 2.4 Selection of the Boundary Conditions at the Coupling Interface

The most common method of coupling 1D-3D code simulations is to decompose the domain into separate regions, while the two codes will model different parts of the system and exchange data at the boundary interfaces, as depicted in Figure 3. In this way the coupled

code system would only require a minimum amount of intrusion into the internal execution processes of the two codes. However, the required parameters for the exchange need to be carefully determined for accurate results and fast convergence. For a fluid-fluid boundary interfaces, the required information arises from the boundary terms of the fluid continuity, momentum, and energy equations. The typical data exchanged at the boundary interfaces include pressure, inlet velocity (or flow rate), and temperature. For fluid-solid boundary interface, the typical data for exchange are the boundary temperature or boundary heat flux.

To obtain valid boundary conditions for both the system code and the CFD code, a common approach is to apply the same set of the boundary conditions (BCs): flow inlet (temperature and velocity) and pressure outlet for both codes, and to send out temperature and flow velocity at the outlet and pressure at the inlet to the other code, as shown in Figure 3. However, if the two-way coupling scheme depicted in Figure 2b or Figure 2c is used, the consistency at the boundary interfaces is not guaranteed (and usually very poor) with this set of data for exchange, and the coupling may lead to an unphysical evolution of the transients. The tight coupling scheme shown in Figure 2d is preferred with this set of BCs.

Another consideration on the selection of data exchange is that some macroscopic parameters need to be conserved at the boundary interface at each time step. If the coupling scheme depicted in Figure 2c or Figure 2d is used, the CFD code will have concurrent BCs from SYS-TH calculation results. Therefore, the temperature and flow information are preferred as the exchange data from SYS-TH to CFD, so that the mass and the energy conservation at the boundary interface is assured. On the other hand, the momentum conservation at the coupling boundary interface is always difficult to achieve since both the SYS-TH and CFD codes usually do not have all the required information to correctly calculate  $\nu \cdot \nabla \nu$  at the interface. The term is usually set to zero at the pressure boundary. This simplification will affect the accuracy of the coupled simulation if there is a significant velocity gradient at the coupling interface.

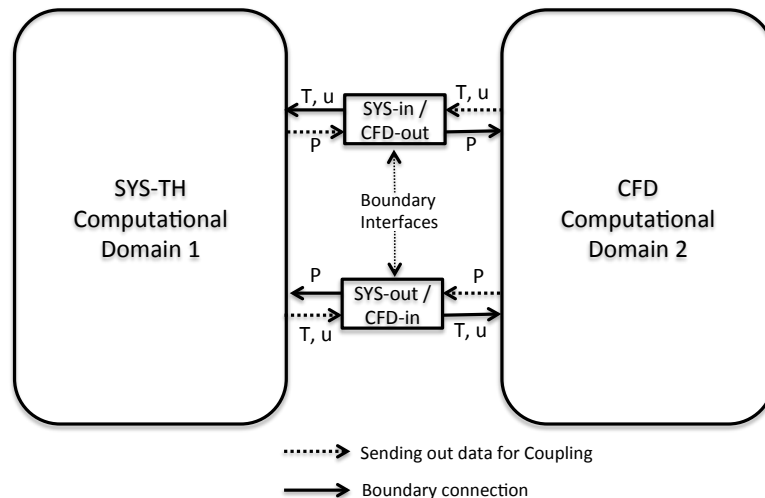


Figure 3: Data Flow for Boundary Coupling

### 3 Coupling Strategy between MOOSE-Based System Codes and STAR-CCM+

The coupling strategy between the MOOSE-based system analysis code for SFR and CFD code STAR-CCM+ is derived based on the discussion in Section 2 and the characteristics of each code.

In order to facilitate the coupling of multi-physics phenomena, MOOSE leverages the finite element library LibMesh and the Jacobian-free Newton-Krylov (JFNK) method in PETSc to solve the coupled nonlinear systems of equations. Thus, the MOOSE-based system codes will solve all the unknown variables simultaneously. It assures the consistency among all variables in the flow field and the thermal field. However, the coupling with a CFD code may only occur at the boundary interface. A domain-overlapping scheme in which the SYS-TH code models the whole domain and the CFD code models one part of the domain, as depicted in Figure 4, will not be suitable. Although parts of the solution vector,  $\vec{x}$ , in the MOOSE-based system code can be overridden (with efforts) by the CFD results at the interfaces, the coefficients of the shape functions in the FEM solutions could remain unchanged; therefore, many internal variables such as the gradients are unchanged.

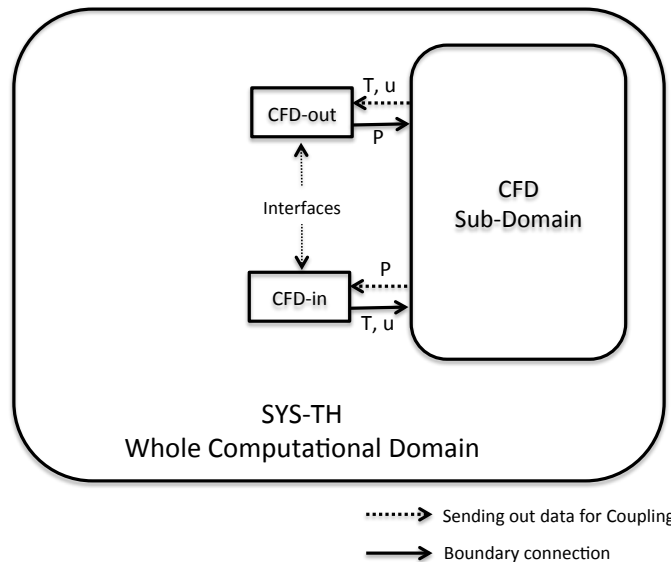


Figure 4: Domain Overlapping Coupling Scheme

Because STAR-CCM+ is a closed-source commercial code, there are some limitations in what coupling schemes can be implemented. In particular, the tight coupling depicted in Figure 2d is not currently possible to implement, since it would require source code modifications to be able to repeat time steps. Therefore, the sequential two-way coupling scheme depicted in Figure 2c was chosen instead. The MOOSE-based system code is the “master” that starts the calculation of a time step by using the interface information from STAR-CCM+ at the previous time step. Then, the results from the system code at this time step are passed to STAR-CCM+ for its iteration. The time step will be advanced once STAR-CCM+ completes its calculation for the time step.



With the sequential coupling scheme, the consistency at the boundary interface is not assured. Therefore the set of BCs shown in Figure 3 will not be suitable. The exchanged information between the system code and STAR-CCM+ are depicted in Figure 5. The system code will receive pressure and temperature information from STAR-CCM+ results, and send out velocity and temperature information to STAR-CCM+ at the boundary interfaces. The boundary interfaces do not need to be specified as inlets or outlets in the system code, and the flow direction will be calculated based on pressure conditions at the boundary. The temperature information at the boundary interface will be used only if fluid flows into the domain of both the system and STAR-CCM+ codes. Using this data exchange scheme, the temperature and flow information at the boundary interfaces are always consistent between the system and STAR-CCM+ codes; and the mass and the energy conservations at the boundary interfaces are assured.

However, the flow-in and flow-out boundary conditions would not be valid for incompressible flow in STAR-CCM+. Once there is a small differences (even round-off error) between the inlet flow and outlet flow BCs, nonphysical results may be produced by the STAR-CCM+ code. In this case, some compressibility needs to be added to the system, either using a compressible flow model, or allowing the volume of the fluid to vary in the STAR-CCM+ calculation. In the case where CFD is modeling a pool with cover gas, this compressibility may be included by modeling the motion of the liquid/gas interface with a volume of fluid model, as was done in the application of SAS4A/SASYS-1 and STAR-CCM+ coupling [12].

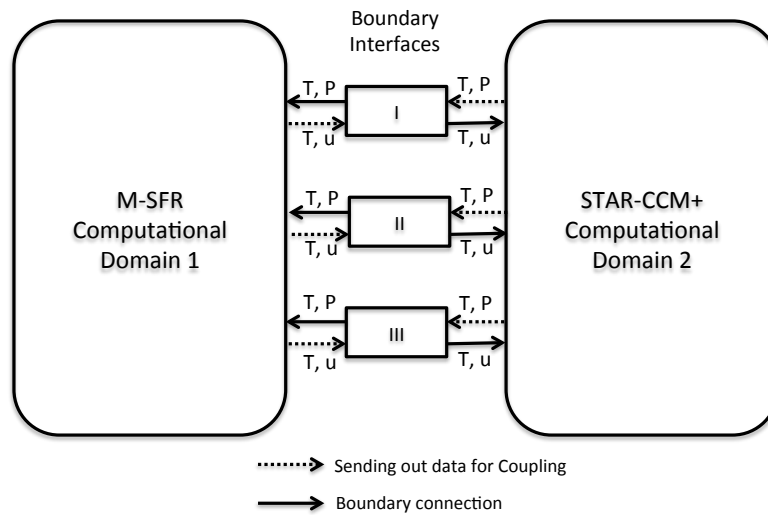


Figure 5: Data Exchange Scheme for the Coupling between the MOOSE-based System Codes and the CFD Code STAR-CCM+

The above strategy developed for the coupling of a MOOSE-based system code and the general CFD code STAR-CCM+ is sufficiently general to be applicable to other multi-scale or multi-physics code coupling applications. However, testing and verification is required before applying to practical problems.

## 4 Implementation of the Coupling Strategy

### 4.1 Implementation in the System Code

As the “master” in the coupled simulation, the system code drives the calculation processes for the coupled code execution. A special MOOSE Executioner, CoupledCFDExecutioner, was developed to implement the coupling strategy between the MOOSE-based system code to the CFD code. It is inherited from the regular Transient Executioner, but with additional processes for communicating with the CFD code at the coupling boundary interfaces. Its process flow chart is depicted in Figure 6, in which the regular processes in a Transient Executioner are on the left, and the dashed lines and blocks on the right are additional processes for the coupled code execution.

Before starting the transient calculation, the system code will configure the boundary interfaces for the coupling, mapping the boundary names in the CFD model and the boundary components in the system code model, defining parameters to be received from or sent to the CFD code, in addition to its normal problem configuration and initiation. A sample input block for the CoupledCFDExecutioner is shown in Figure 7 in which the coupling boundary component names, their names in the CFD model, the input and output parameters, and the data exchange files are defined.

At each time-step, the system code will read in the CFD simulation results at the coupling boundary interface, complete its own inner iterations for the time-step, and then send out its results at the boundary interfaces to the CFD code for its calculation at this time-step. This is the same process shown in Figure 2c. Once the transient simulation in the system code is completed, it sends out a signal to terminate the CFD code calculation.

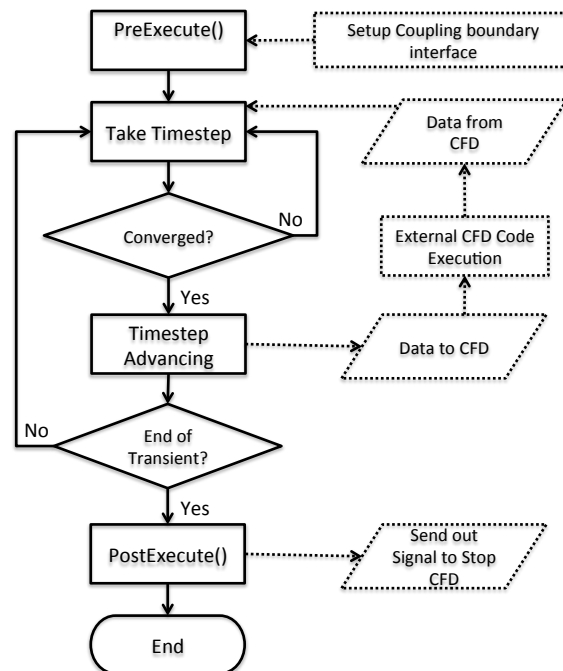


Figure 6: Execution Process Flow Chart of the CoupledCFDExecutioner

```
[Executioner]
type = CoupledCFDExecutioner

input_data_file = CFDTOSYS.csv
n_in_parameter = 4
name_of_in_components = 'tank_outlet tank_outlet tank_inlet tank_inlet'
names_of_CFD_boundary = 'Outlet Outlet Inlet Inlet'
name_of_in_parameters = 'p_bc T_bc p_bc T_bc'

output_data_file = SYSTOCFD.csv
n_out_parameter = 4
name_of_out_components = 'tank_outlet tank_outlet tank_inlet tank_inlet'
name_of_out_parameters = 'massflow temperature massflow temperature'
... ..
[]
```

Figure 7: Sample Input Block for the CoupledCFDExecutioner

#### 4.2 Implementation in STAR-CCM+

The implementation of the coupling strategy into the CFD code is performed via Java macros that operate on the STAR-CCM+ client, similar to the approach taken when coupling with SAS4A/SASSYS-1 [12]. With STAR-CCM+, a Java API is provided that enables the user to modify the code's client, i.e. user interface, thus providing a mechanism to exchange boundary condition data with the system code each time step.

The system code is considered to be the “master” process in the coupled simulation, and therefore dictates the time step size. Along with boundary condition data, the system code transmits the current time step size, and the macro adjusts the CFD time step size accordingly.

Each flow boundary in the STAR-CCM+ model is associated with two so-called “field functions”, one that provides the velocity boundary condition and one that provides the temperature boundary condition. After reading updated boundary condition data from the system code, the macros modify the definition of these field functions. Currently, these field functions are defined by single values in order to apply uniform velocity and temperature at each boundary, but the field functions may be used to provide some distribution. STAR-CCM+ provides functionality, through what it calls “reports”, to calculate various integrals and averages of the solution data. In order to calculate the boundary pressure for the CFD code, a surface-average report is defined for each flow boundary. Similarly, the temperature is calculated by mass flowrate-averaged reports associated with each flow boundary. These field functions and reports follow a simple naming convention, e.g. the field function associated with the temperature boundary conditions at a particular boundary is named “InletBC\_T\_” followed by the name of the boundary. The user must create these field functions and reports prior to running the coupled simulation. However, a separate set of macros has been created to automate this process.

The macro is also responsible for publishing the CFD results during the transient. The history of the boundary condition data transferred to and from the CFD code is printed to text

log files. Furthermore, image files are periodically generated to provide visualizations of the 3-D flow field and temperature profiles as they evolve during the transient. Backup files of the CFD simulation results are also generated periodically, which are synchronized with backups of the system code's restart file.

The function of the Java macros during the coupled simulation is to receive the boundary condition data and the time step size from the system code, update the field functions associated with each boundary, update the time step size, run one time step, run reports to calculate averaged quantities at each boundary, send the averaged boundary data to the system code, publish results, and wait for the system code to complete its time step.

## 5 Demonstration of the Coupling Strategy

### 5.1 Description of the Test Problems

A simple test problem was developed to examine the coupling strategy and its implementation in the system code and CFD code. The flow loop of the test problem is shown in Figure 8, which consists of one tank, one pump, and four pipes. In the coupled calculation, the tank, with cover gas, will be modeled by STAR-CCM+, while the rest of the loop will be modeled by the system code. The details of the models for each code will be discussed next.

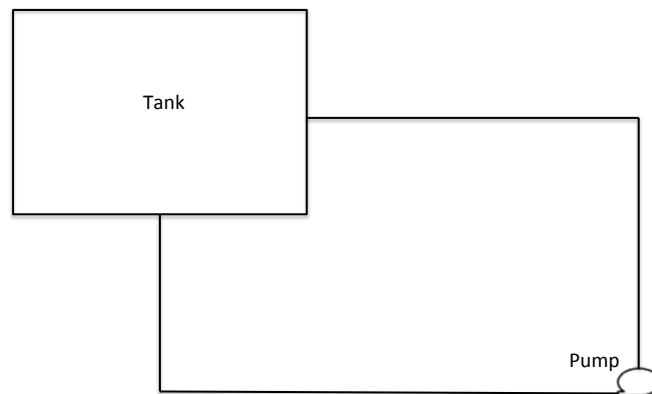


Figure 8: Schematics of the Test Problem

The coupling strategy has been demonstrated by the following tests: (1) Steady-State Simulation; (2) Flow Transient; and (3) Temperature Transient. The details of the tests and their results will be discussed.

#### 5.1.1 System Model of the Loop

The loop models of the system code are shown in Figure 9 for both the coupled code simulations and the stand-alone system code simulations. In the coupled code simulation model, the loop is closed by two 0-D boundary components since the tank is modeled by the CFD code. In the stand-alone simulation model, the tank is modeled by a 0-D VolumeBranch component in which a perfect mixing model is implemented. An additional boundary component (TDV) is added in the model to provide a reference pressure in the stand-alone system code simulations. The components and related parameters in the loop model are listed

in Table 1. The working fluid in the test problems is sodium, and a sodium Equation of State model has also been developed based on the RELAP-7 non-isothermal equation-of-state model and the sodium property correlations in SAS4A/SASYS-1.

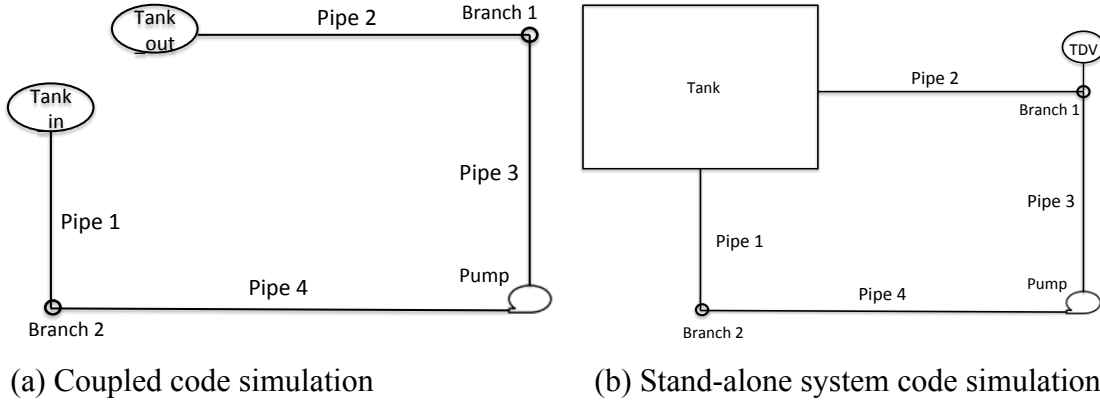


Figure 9: The Loop Model in the System Code

Table 1: Component Parameters of the Test Loop Model in System Code

Component	Type	Flow Area (m <sup>2</sup> )	Hydraulic Diameter (m)	Length (m)
Pipe 1	Pipe	0.0314	0.2	1
Pipe 2	Pipe	0.0314	0.2	2
Pipe 3	Pipe	0.0314	0.2	1.6
Pipe 4	Pipe	0.0314	0.2	2.6
0-D Components	Type	Flow Area (m <sup>2</sup> )	Volume (m <sup>3</sup> )	Notes
Pump	PresetPump	0.0314	-	Pump head depends a pre-defined function
Branch 1	VolumeBranch	0.0314	$3.14 \times 10^{-6}$	$K_{in} = K_{out} = 100$
Branch 2	VolumeBranch	0.0314	$3.14 \times 10^{-6}$	$K_{in} = K_{out} = 0$
Tank_in	TimeDependent-Volume	-	-	Pressure and temperature from CFD
Tank_out	TimeDependent-Volume	-	-	Pressure and temperature from CFD
Tank	VolumeBranch	0.0314	0.67415	The same tank volume as the CFD model
TDV	TimeDependent-Volume	-	-	Provide reference pressure in stand-alone simulation

### 5.1.2 CFD Model of the Tank

The CFD model solves the transport equations for mass, momentum, and thermal energy of the coolant tank. The implicit unsteady model is employed to predict time-sensitive conditions using a stable solver. The tank coolant includes both the primary sodium coolant and cover gas. The two phases are modeled using the volume-of-fluid approach, which is

applicable for modeling immiscible fluids where the two phases may be approximated to share a common velocity, pressure, and temperature field. In this case, including a model of the cover gas allows the level of the sodium/gas interface to move during the transient, thus providing the necessary compressibility to permit the system code to specify the flow rate at all flow boundaries. The temperature dependence of the sodium density and thermal conductivity is treated using the same polynomials available in SAS4A/SASSYS-1 [5]. The cover gas is argon and is treated as an ideal gas. Turbulence is modeled using the Realizable  $k$ - $\epsilon$  model with all- $y^+$  wall treatment. The Realizable  $k$ - $\epsilon$  model is one of several Reynolds-Averaged Navier Stokes (RANS) models available in STAR-CCM+ and has shown success in a wide range of flow conditions and has been used in past analyses of the Monju upper plenum [15] and EBR-II cold pool [12]. Segregated, rather than coupled, solvers were employed for the coupling of the iterative solution of the flow, energy, VOF, and turbulent transport equations, based on success of earlier models. In order to improve convergence, tight tolerances were applied to the inner sweeps of the momentum and turbulent kinetic energy transport equations. Furthermore, ten inner iterations were performed per time step rather than the default five iterations.

The tank has a relatively simple geometry, shown in Figure 10, with the values of the geometric parameters in Table 2. The main body of the tank is a cylinder with height and inner diameter of 1.0 m. Flow enters through a pipe at the bottom of the tank and exits through a horizontal pipe attached at one wall. The axis of the horizontal outlet pipe is positioned halfway between the top and bottom surfaces of the tank, at  $z_{\text{out}} = 0.5$  m. The liquid/gas interface is initially at an elevation of 0.85m, which provides some margin to avoid gas exiting through the outlet pipe. Rounded protrusions were created for both the inlet and outlet junctions, and are considered part of the tank domain. The length of the connecting junction between the inlet pipe and the bottom of the tank is 0.1 m and its radius of curvature is also 0.1 m. The protrusion from the tank to the outlet pipe is 0.05 m long and also has a radius of curvature of 0.1 m.

A base mesh size of 0.01 m was employed with 3 layers of prismatic cells along the walls, yielding a total of 300k cells. The trimmer mesher was employed for the core mesh, which generates hexahedral cells except where cells are “trimmed” at boundary surfaces. The hexahedral cells are oriented such that each cell has a pair of faces orthogonal to each coordinate direction. Thus cells in the vicinity of the liquid/gas interface have two pairs of faces normal to the interface. The mesh can be seen in the views in Figure 11. A formal mesh convergence study has not yet been performed for the test model. Unfortunately, about 1/3 of the fluid adjacent to the tank sidewall is in the  $y^+$  range ( $8 < y^+ < 20$ ) where neither the low nor high Reynolds wall treatment is valid. However, for the purposes of providing a test problem to demonstrate the coupling capability, accuracy of the near-wall turbulence models was not a high priority and the models will be refined in the future. A constant time step size of 0.01 s was employed. Although no formal study was performed, results with the default 0.001 s time step size did not differ appreciably from the 0.01 s results.

Velocity inlet boundary conditions are applied to both flow boundaries. At a velocity inlet boundary, a specification of both temperature and velocity must be provided, along with turbulent intensity, turbulent viscosity ratio, and the volume fractions of the liquid and gas phases. Despite the name, it is not necessary to provide inward-directed flow at an inlet boundary, and in fact outward-directed flow is specified for the outlet. In the case of outward-

directed flow, the solvers ignore the specified values of the temperature, turbulence, and volume fraction. For the steady-state initialization, a uniform velocity and temperature profile were assigned to the true inlet boundary of 0.5 m/s and 625K. At the outlet boundary, the specified velocity is nearly 0.5 m/s, but was adjusted slightly to account for the difference in the flow area caused by meshing. The adjusted outlet velocity was 0.5003 m/s. The values of velocity and temperature will be updated by the system code during the coupled analyses.

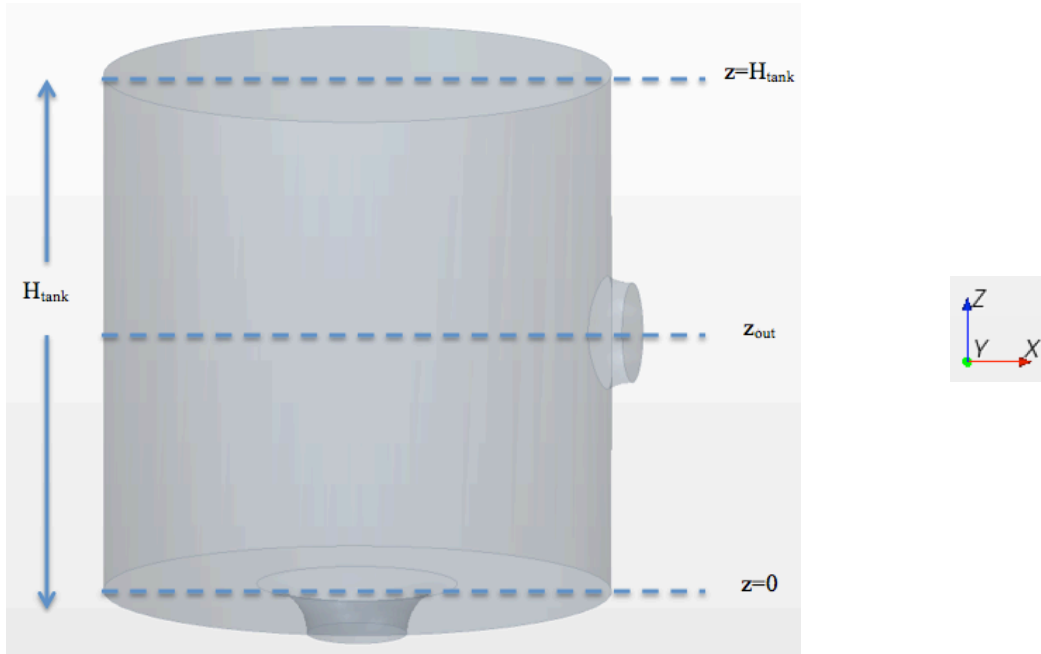


Figure 10: Side View of the STAR-CCM+ Geometry for the Test Problem

Table 2: Geometry of the Test Tank Model in STAR-CCM+

Parameter	Description	Value (m)
$D_{\text{tank}}$	Inner diameter of the main tank	1.0
$H_{\text{tank}}$	Height of the main tank	1.0
$z_{\text{out}}$	Elevation of the outlet pipe centerline, relative to the bottom of the main tank	0.5
$D_{\text{in}}$	Inner diameter of the inlet pipe (at its narrowest)	0.2
$D_{\text{out}}$	Inner diameter of the outlet pipe (at its narrowest)	0.2

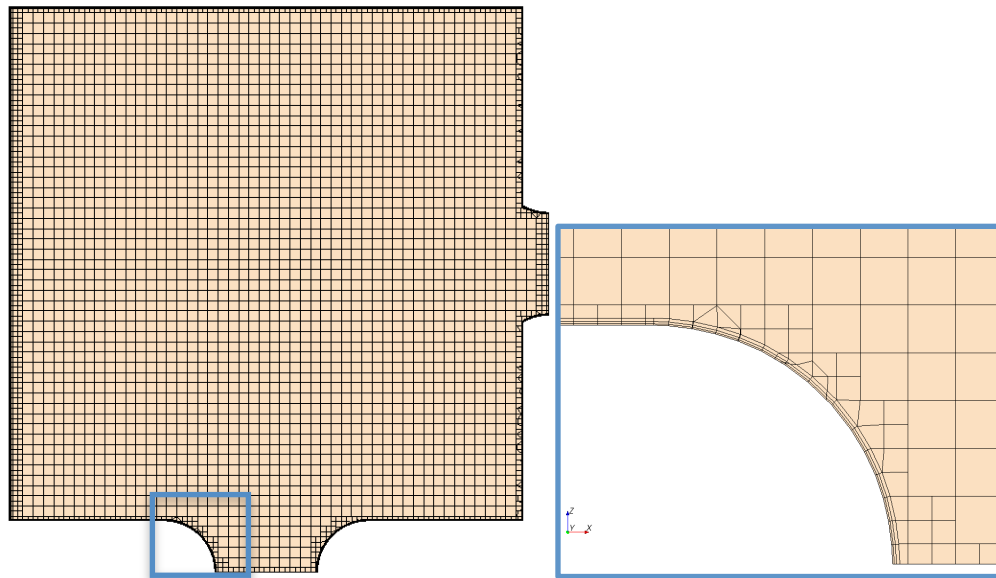


Figure 11: CFD Mesh on the Vertical Plane Slicing through the Centers of the Inlet and Outlet Boundary Surfaces: Entire Plane (left) and Vicinity of the Inlet Junction (right)

## 5.2 Steady-State Simulation Results

In order to initialize the CFD calculation, a standalone STAR-CCM+ calculation was performed with boundary conditions consistent with the coupled calculation. This calculation employed the unsteady solvers, as required by the VOF model, but the boundary conditions were held fixed. The simulation was run off-line for more than 1 minute, in order to achieve an equilibrium condition. This was followed by a 5-second coupled simulation where there is no change in the loop (either in the heat or momentum sources) to ensure that a stable steady state is reached prior to the flow and temperature transient calculations.

The velocity field evolved from a condition with zero velocity to the equilibrium condition that features a jet dissipating into the tank, accelerated flow near the outlet junction, and recirculation in the region far from both flow boundaries (see Figure 12). In the gas region just above the interface, there are small recirculation regions where the velocity is predicted to exceed 1 m/s. From Figure 13, the liquid/gas interface is relatively flat, but does expand in the center due to the influence of the jet. The interface is diffused across 3 mesh cells, a distance of 0.06 m, due to mesh resolution and numerical diffusion. The sharpness of the interface should be improved in future work, but the interface dynamics are not important to the current demonstration problem. The absolute pressure field is provided in Figure 14. The pressure profile exhibits a relatively uniform gradient, as gravity is the primary influence. At the end of the coupled steady state initialization, the difference in the absolute pressure averaged over the inlet and outlet surfaces was predicted to be 5200 Pa. The initial temperature in the tank was set to 623K, 2K below the inlet temperature, in order to gauge the rate of convergence of the transient towards equilibrium. After one minute, some coolant in the relatively stagnant regions has not yet been warmed (or replaced) by the sodium from the inlet jet. However, the 2K temperature difference is not significant for the purposes of this analysis, and so the coupled simulation was permitted to proceed.



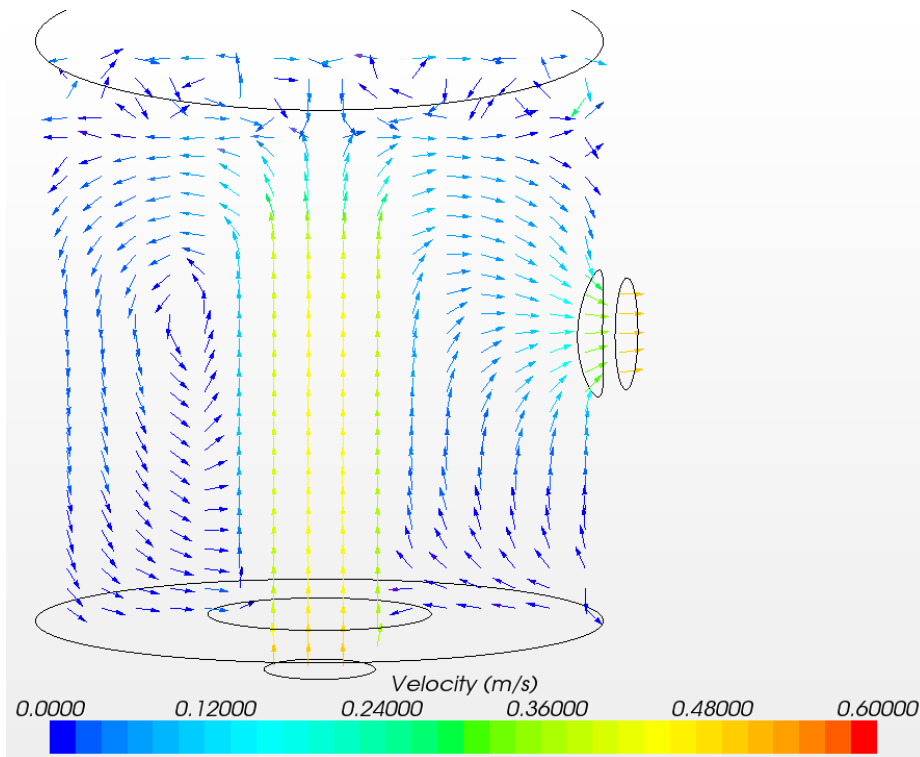


Figure 12: CFD Prediction for the Velocity Field at the Initial Condition at the Vertical Plane Slicing through the Centers of the Inlet and Outlet Boundary Surfaces

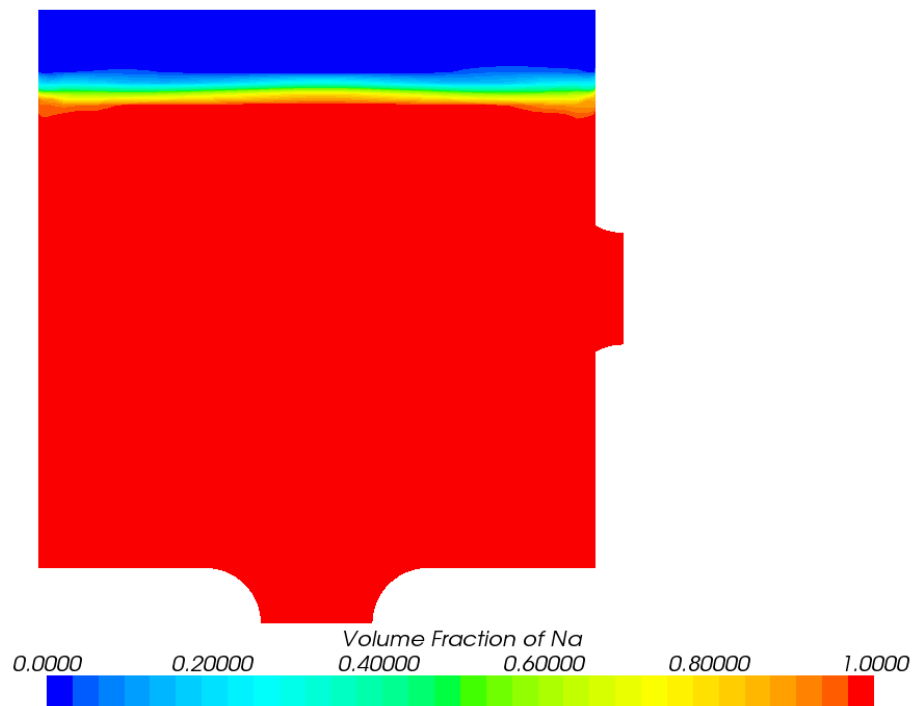


Figure 13: CFD Prediction for the Sodium Volume Fraction at the Initial Condition at the Vertical Plane Slicing through the Centers of the Inlet and Outlet Boundary Surfaces

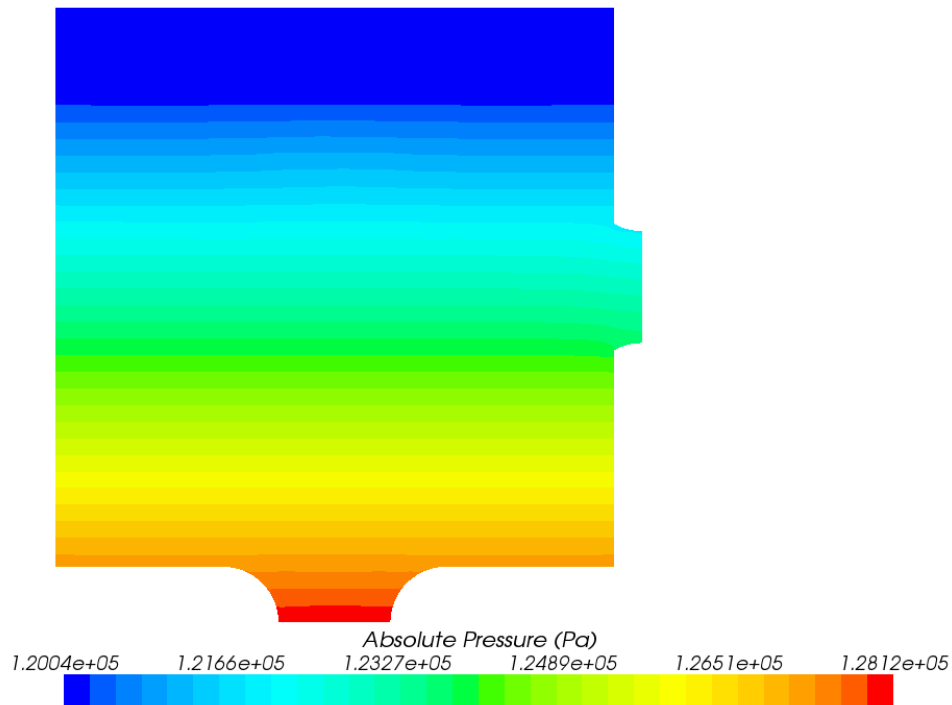


Figure 14: CFD Prediction for the Pressure at the Initial Condition at the Vertical Plane Slicing through the Centers of the Inlet and Outlet Boundary Surfaces

A stand-alone system code calculation, using the model depicted in Figure 9b, has also been performed to examine the differences and consistency between the coupled code and standalone system code simulations. Figure 15 shows the calculated pressure fields in the standalone simulation. The pressure profile shows a clear trend of higher pressure at lower positions since the gravity is dominant in the simulation. Sudden pressure decreases are also present across a flow branch (circled in Figure 15) as a result of large local form losses. The pump, on the contrary, serves as momentum sources in the loop and therefore a sudden pressure increase is observed across the pump. The pressure differences between the tank inlet and tank outlet is 5099 Pa in the standalone simulation, while it is 5201 Pa in the coupled simulation. This is because the friction pressure loss is ignored in the current VolumeBranch model, and the form loss is assumed zero in this test problem. The differences in the pressure drop caused slightly different (0.24%) velocity predictions in the two simulations, 0.4987 m/s in coupled simulation vs. 0.4999 in the standalone simulation. Uniform velocity distributions are expected in both simulations since all four pipes have the same diameter. The differences in the two simulations can be easily removed by providing adjusted form loss coefficients in the standalone system code model. In fact, CFD simulation is the right tool to generate the proper value of the local form loss coefficient (also known as the K-factor) because of the difficulties to estimate the effects of not-fully developed flow and to separate the irreversible pressure drop from the experimental data.

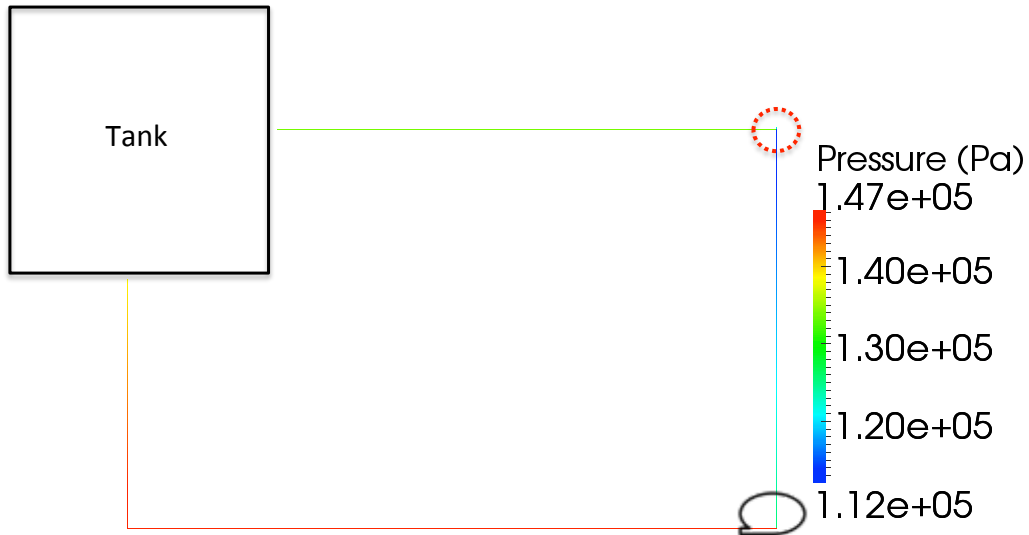


Figure 15: Pressure Distributions in the loop of the Stand-alone Steady-State Simulation

### 5.3 Flow Transient Simulations

A postulated flow transient was developed to examine the coupling strategy. A pre-defined time-dependent pump head, shown in Figure 16, is applied in both the coupled code and the stand-alone system code simulations, starting from their respective steady states discussed above.

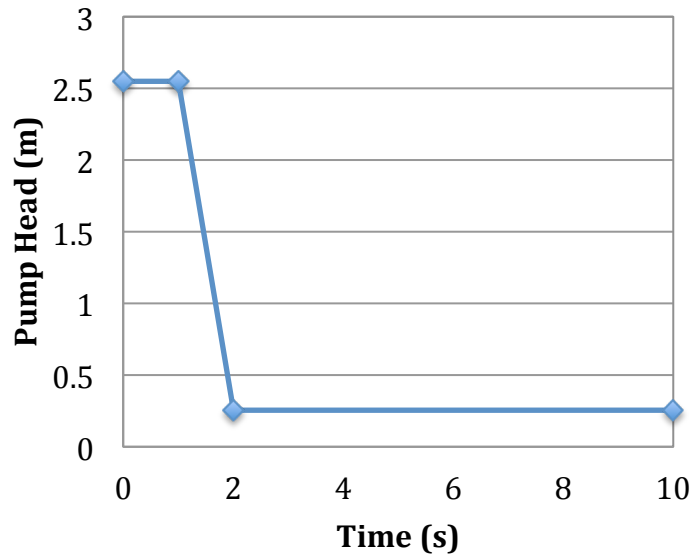


Figure 16: Pre-defined Pump Head during the Flow Transient

The CFD simulation predicts the diminishing influence of the jet in the tank as time progresses following the reduction in flow rate. Due to the inertia of the sodium in the tank interior, the peak velocity occurs far from the tank inlet during the intermediate stage of the

transient ( $2 \text{ s} \leq t \leq 4 \text{ s}$ ), as can be seen in the velocity magnitude profiles in Figure 17. After 6 seconds, the profile is restored to the typical jet structure, albeit at a reduced flow rate. The predictions of the liquid volume fraction profile (see Figure 13) initially exhibit a swell in the vicinity of the jet. Over the course of the pressure transient, this swell is reduced and the liquid/gas interface flattens.

In the stand-alone system code simulation, uniform velocity distributions are observed since all four pipes have the same diameter and the compressibility of the sodium is insignificant. Although the pump head stays unchanged for the first two seconds of the transient, the flow velocities in the loop keep decreasing due to inertia, shown in Figure 18. The tank inlet velocities in both the stand-alone system code and coupled code simulations are shown in Figure 18. The differences are very small during the entire transient, only slightly higher than the difference in the steady-state results (0.24%). This is expected since a 0-D or 3-D representation of the tank has negligible effects to the pressure wave propagation.

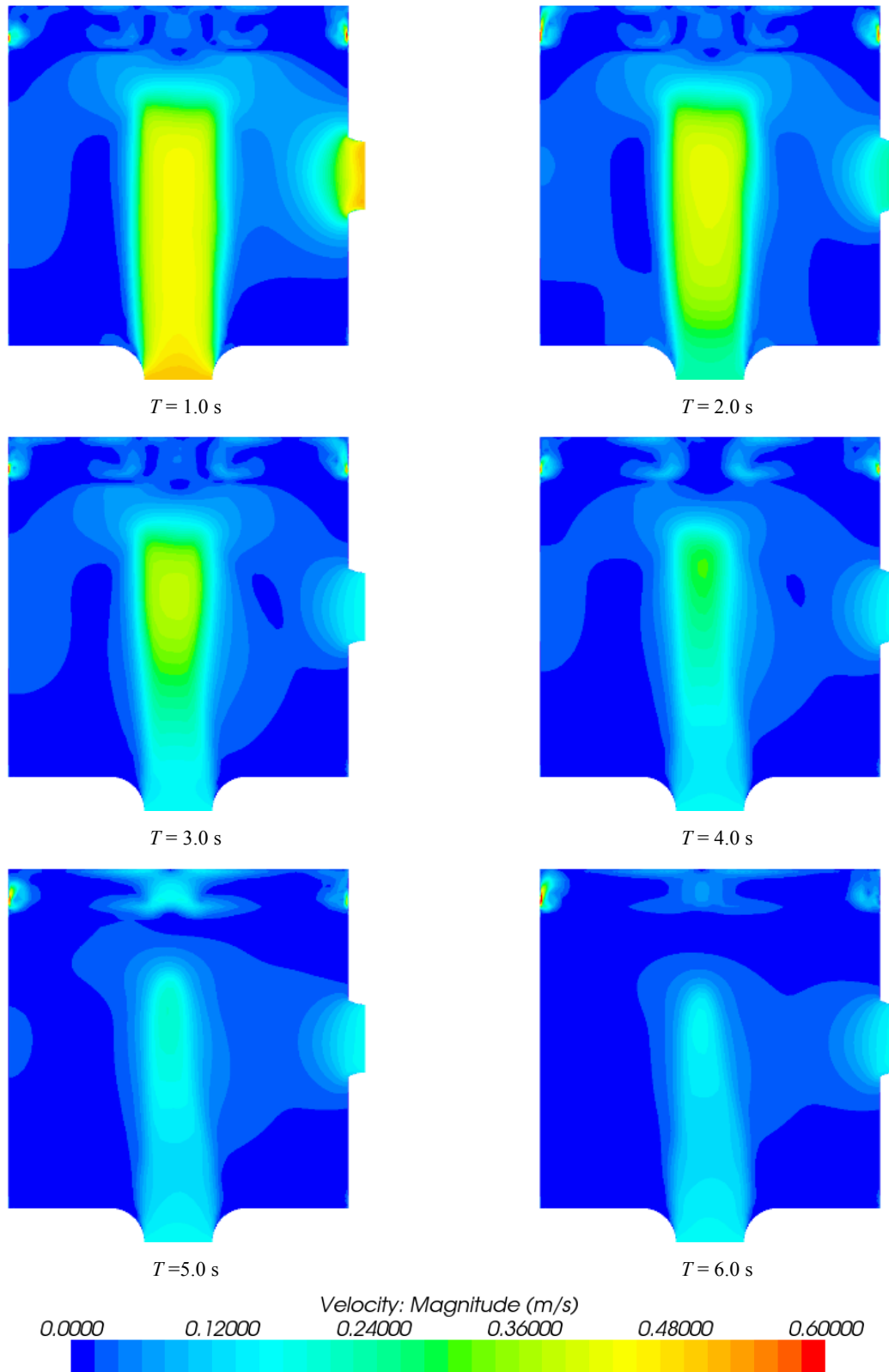


Figure 17: CFD Prediction for the Velocity Profile Evolution during the Flow Transient

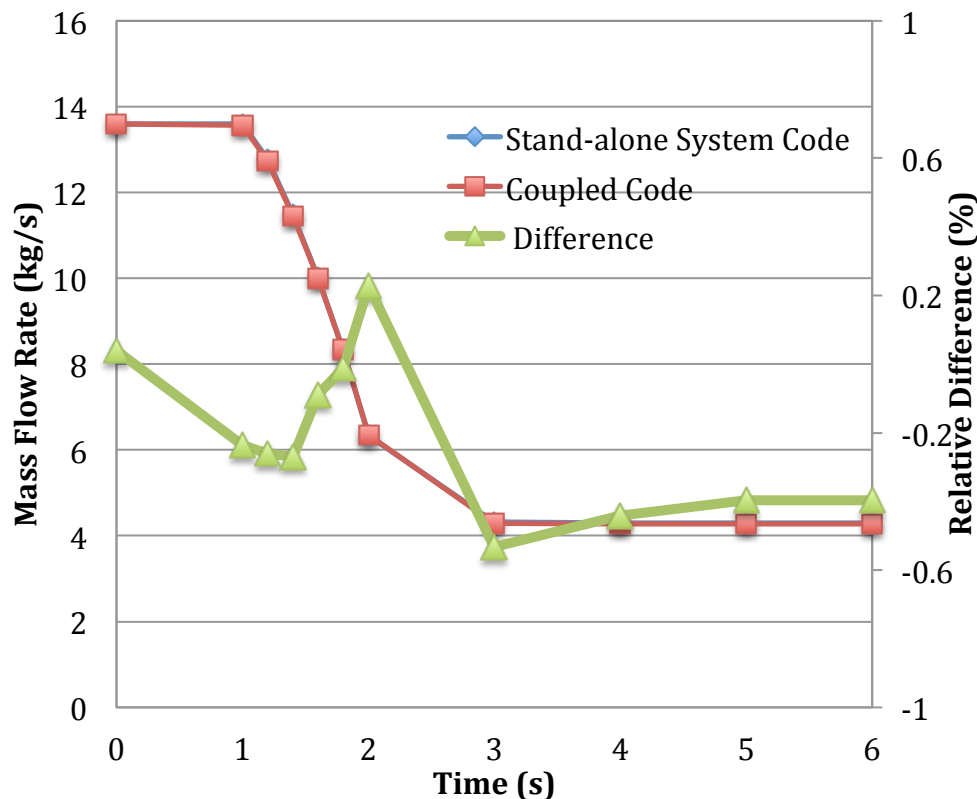


Figure 18: Comparison of Mass Flow Rates at Tank Inlet during the Flow Transient

#### 5.4 Temperature Transient Simulations

A postulated temperature transient was developed to examine the effects of thermal stratification in a large tank and to demonstrate the significance of the coupled multi-scale simulation. The temperature transient is divided into two stages:

- (1) Cooling of tank inlet pipe (Pipe 1 in Figure 9) for 7.5 seconds;
- (2) 300 seconds adiabatic simulation of the non-isothermal flow after Stage 1.

In the hypothetical cooling stage, the pipe connected to tank inlet is cooled by a heat sink with fixed temperature at 525 K and fixed convective heat transfer coefficient of  $10^4 \text{ W/m}^2 \cdot \text{K}^{-1}$ . Both the coupled code and the stand-alone system code simulations have been performed, starting from their respective final steady-states after the flow transient discussed in Section 5.3.

##### 5.4.1 Cooling Transient Results

The temperature distributions in the tank during the cooling transient are shown in Figure 19 for the coupled code simulation. Strong thermal stratification in the tank is observed in the coupled simulation. The tank inlet temperature dropped very fast while the outlet temperature stays unchanged. In the stand-alone system code simulation, the decrease of the tank outlet temperature is small but noticeable during the transient, as shown in Figure 20. This is because the flow rate is small and the cooling transient is short, but the volume of the tank is

large. The average temperature of the tank only changes from 625K to 622.65K at the end of cooling transient in the stand-alone system code simulations.

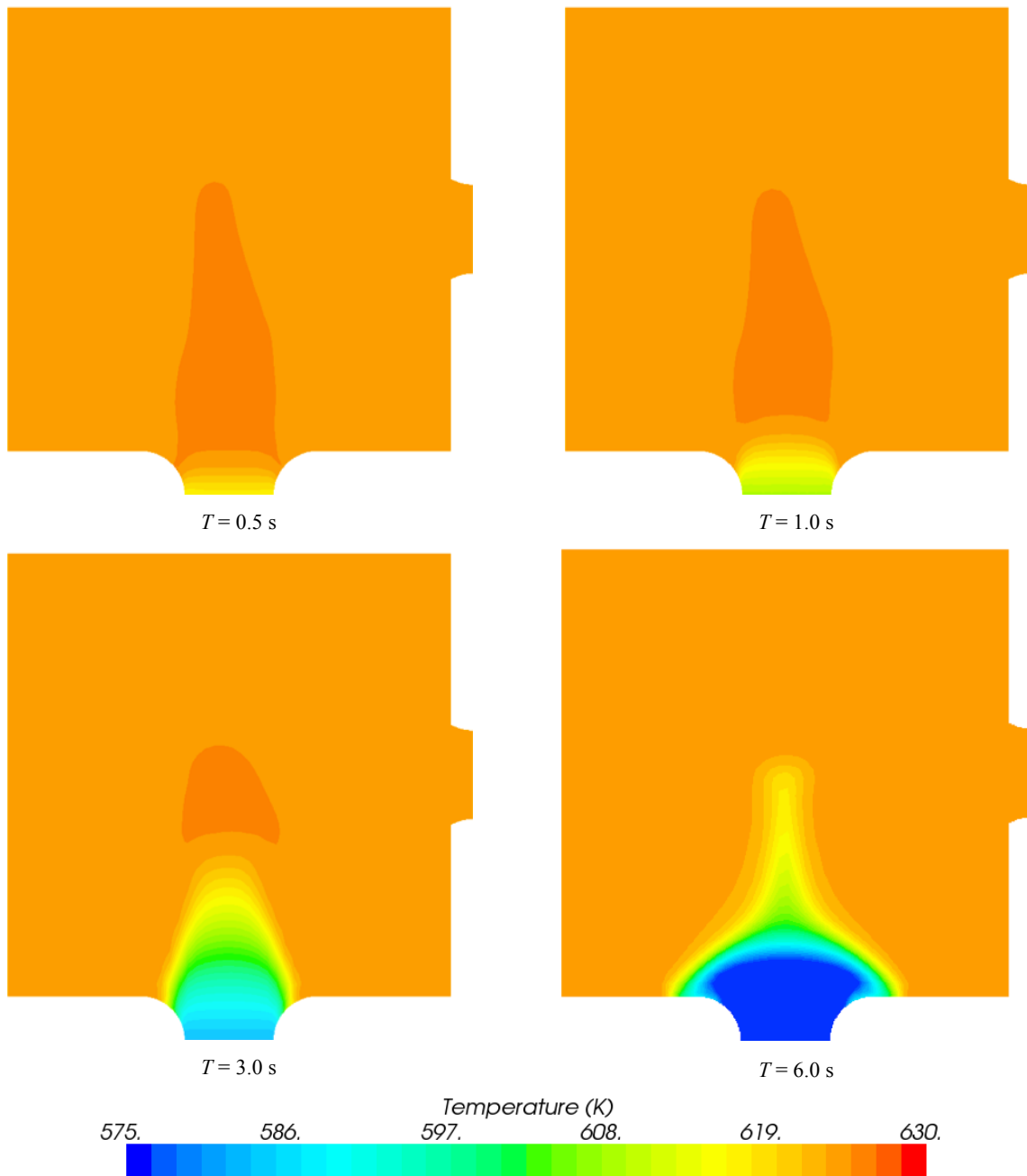


Figure 19: CFD Prediction for the Temperature Evolution during the Cooling Transient

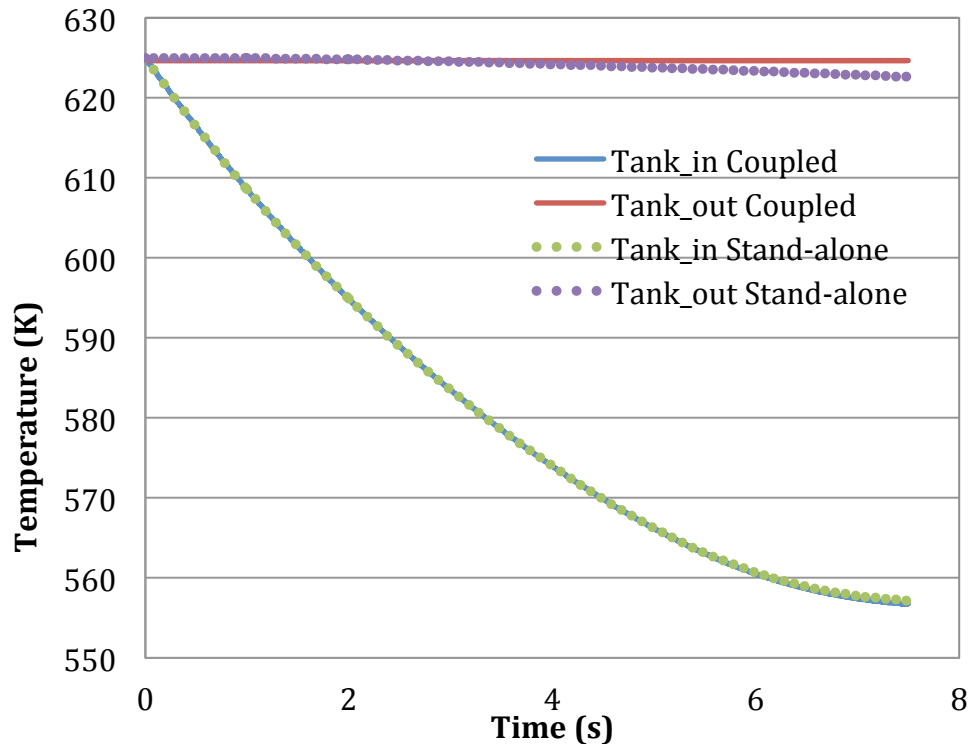


Figure 20: Comparison of Tank Inlet and Outlet Temperature during the Cooling Transient

#### 5.4.2 Non-Isothermal Flow Approaching Steady-State

At the end of cooling transient, the simulations were continued to allow the unsteady non-isothermal flow to approach a new steady state. The evolution of temperature distributions in the tank during the transient are shown in Figure 21 for the coupled code simulation. Note that the time was reset to zero at the end of cooling transient. Strong thermal stratification in the tank is observed. The tank inlet temperature starts increasing right after the cooling transient since the rest of the loop (except Pipe 1) remains very hot. The tank inlet temperature responses are almost the same for the first 30 seconds of the transient in both the coupled code and stand-alone system code simulations, as seen in Figure 22. The tank outlet temperature responses from the two simulations are very different due to the thermal stratification in the tank, as shown in Figure 21. In the coupled code simulation, the tank outlet temperature remains unchanged for about 15 seconds, and then decreases very slowly during the entire transient. In the stand-alone system code simulation, the tank outlet temperature quickly drops in about 6 second (time for the flow to pass through Pipe 1), and then slowly approaches to a steady-state value at about 120 second, where both the tank inlet and outlet temperatures stabilize at the same value in Figure 23. In the stand-alone system code simulation, the tank inlet temperature quickly increases after the cooling transient, exceeds the tank outlet temperature, and then drops below the tank outlet temperature. This pattern repeats as the solution approaches the final steady state. The similar transient response is not observed in the coupled code simulation.

The temperature distributions in the loop are shown in Figure 24 ( $T = 2s$ ) and Figure 25 ( $T = 20, 40, \text{ or } 300 s$ ) for both the coupled code and the stand-alone system code



simulations. At  $T = 2s$ , the temperature distributions of the loop are similar in the two simulations, except that slightly lower temperature were predicted for the first a few nodes of Pipe 2 (connected to tank outlet) in the stand-alone system code simulations due to lower temperature predictions at the tank outlet. The temperatures of Pipe 1 (connected to tank inlet) start increasing once the cooling transient ends. At  $T = 20s$ , the temperatures at all nodes of Pipe 1 are at about 625 K because the upstream hot fluid has travelled here in both simulations. The temperature distributions in other pipes (Pipe 2-4) are quite different in the two simulations because of the different predictions of tank outlet temperature over time. The total length of the four pipes is 7.2 meters, and it takes 45.6 seconds for the fluid move from the tank outlet to the tank inlet. It is observed in Figure 25 that the higher temperature fluid in Pipe 3 and Pipe 4 at  $T = 20s$  has flowed into Pipe 1 at  $T = 40s$ . At  $T = 40s$ , the temperature predictions of all four pipes in the stand-alone system code simulation are lower than the coupled code predictions. At  $T = 300s$ , the system is at its final steady state in the stand-alone system code simulation. However, it has not approached its new steady state in the coupled code simulation. Although temperature predictions in the four pipes are almost the same, large temperature differences still exist in the tank due to the thermal stratification, as shown in Figure 26.

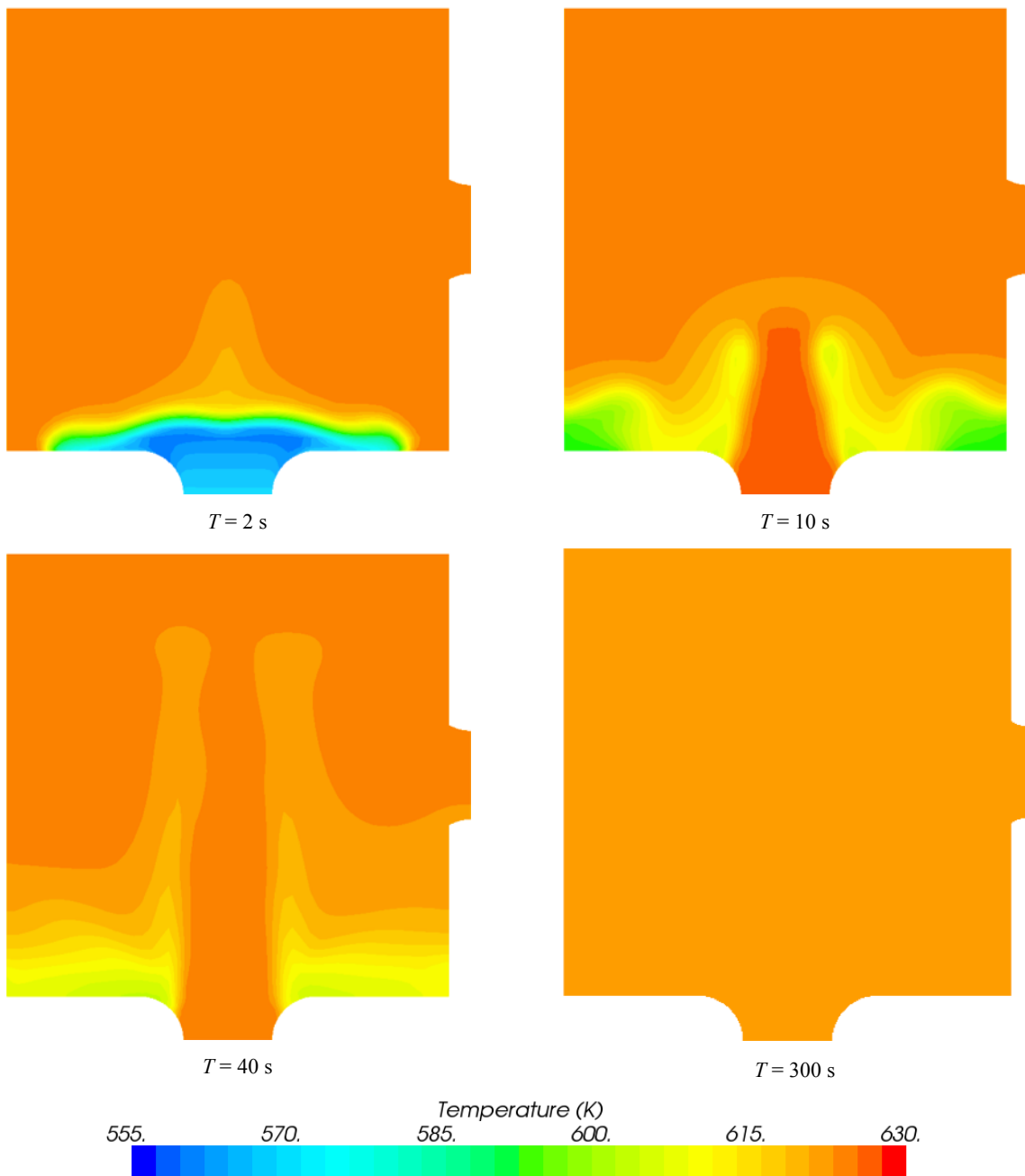


Figure 21: CFD Prediction for the Temperature Evolution after Cooling Transient

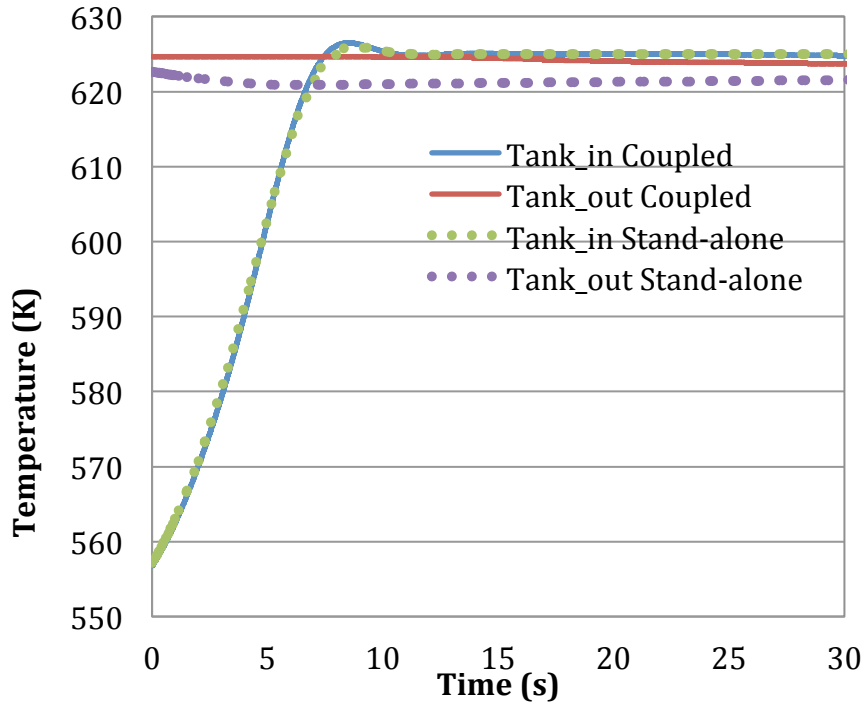


Figure 22: Comparison of Tank Inlet and Outlet Temperature during the Temperature Transient after Cooling,  $T = 0 - 30$  s

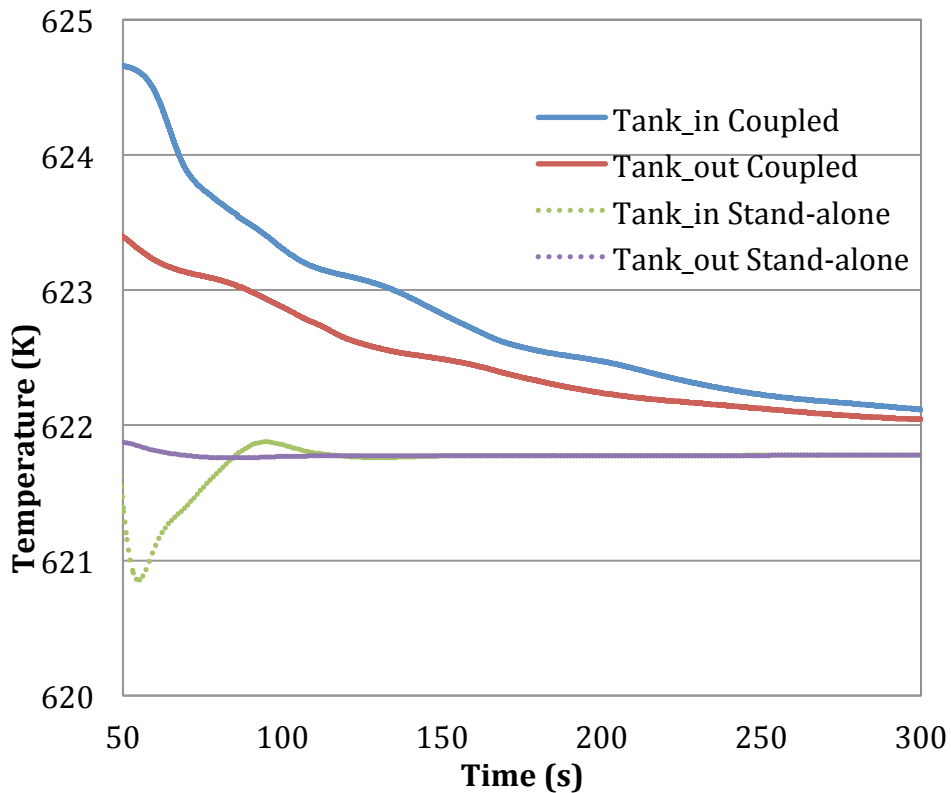
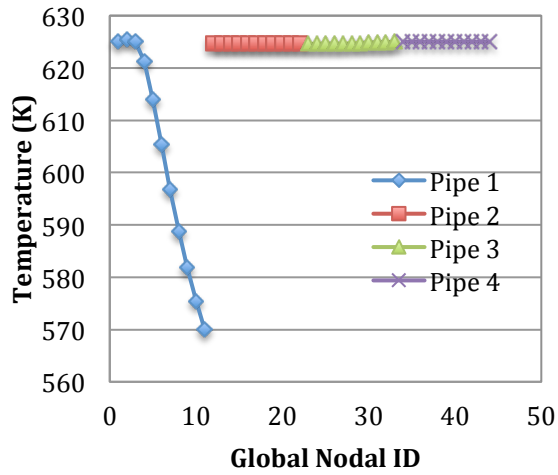
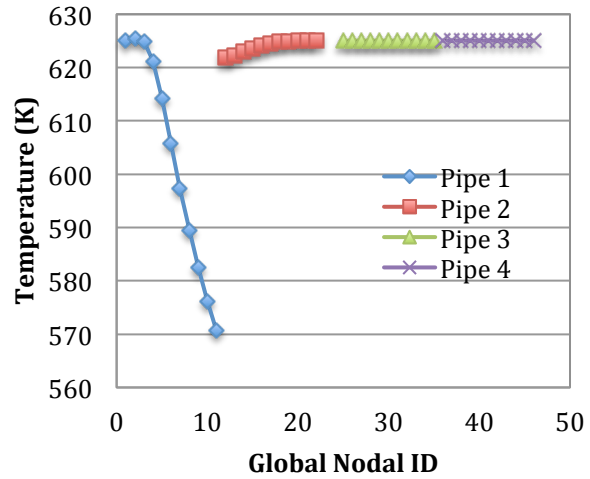


Figure 23: Comparison of Tank Inlet and Outlet Temperature during the Temperature Transient after Cooling,  $T = 30 - 300$  s

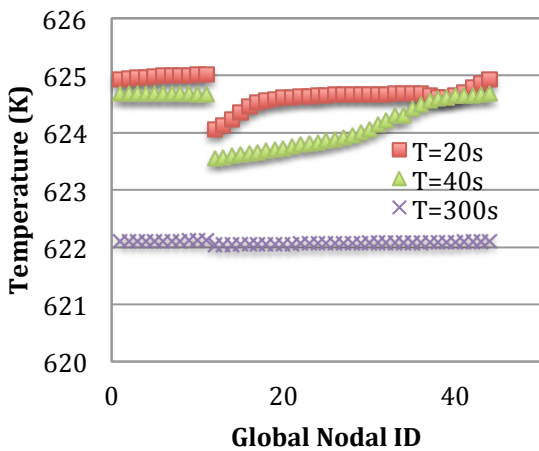


(a) Coupled Code

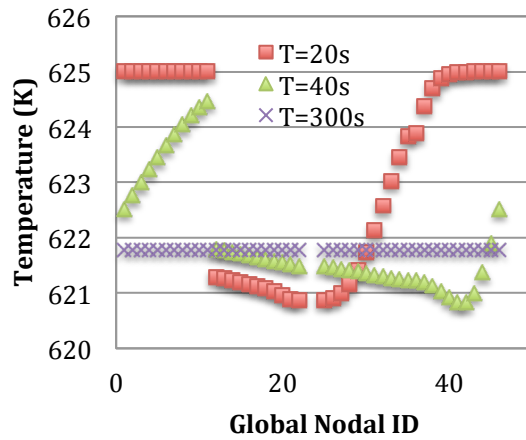


(b) Stand-alone System Code

Figure 24: Temperature Distribution of the Loop System,  $T = 2$  s

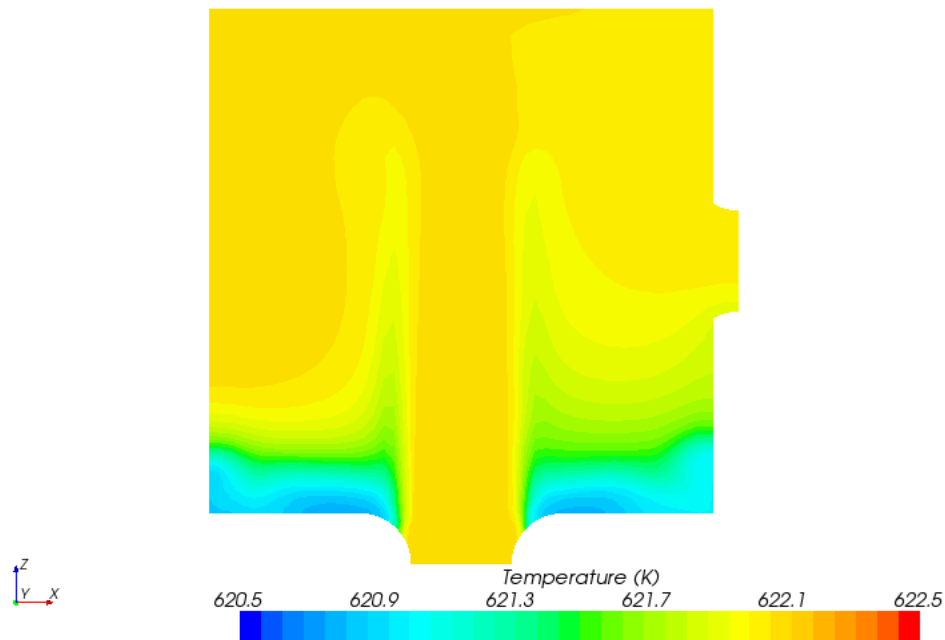


(a) Coupled Code



(b) Stand-alone System Code

Figure 25: Temperature Distribution of the Loop System,  $T = 20, 40, \text{ or } 300$  s



Time = 300 (s)

Figure 26: CFD Prediction of the Temperature Distribution in the Tank,  $T = 300s$

## 6 Summary and Future Work

The multi-scale single-phase flow coupling strategy is investigated in this work in the context of a MOOSE-based system code and the commercial CFD code STAR-CCM+. This work is extended from the earlier work with the coupling of the SAS4A/SASSYS-1 system code and the CFD codes STAR-CD and STAR-CCM+. This investigation is important to the integration between the MOOSE-based system code and the high-fidelity and medium-fidelity advanced simulation capabilities developed under the NEAMS RPL. The general code-to-code coupling issue, and various options for the coupled multi-scale single-phase flow simulations were discussed. The coupling strategy for the MOOSE-based SFR system analysis code and STAR-CCM+ has been selected and implemented. The developed strategy is sufficiently general to be applicable to other multi-scale or multi-physics code coupling applications.

The coupling strategy has been demonstrated by several test cases of a simple flow loop model, for which a CFD model of a large tank is coupled to a systems model of the remaining hydraulic pipe loop. Reasonable results of steady state, flow transient, and temperature transient have been obtained from both the coupled code and the stand-alone system code simulations. Very different system responses were observed during the temperature transient test between the coupled code and the system code simulations because the strong thermal stratification in the tank can only be accurately modeled in the coupled code simulation. These preliminary results provided a proof-of-principle of the coupling strategy between the system code and the CFD code, and demonstrated the significance of the coupled multi-scale simulation. In particular, the similar behavior of thermal stratification in the outlet plenum of a SFR would influence the behavior of the primary coolant system in the natural circulation

regime. The transient behavior of the reactor would be significantly different when comparing the predictions of the coupled CFD model to the simpler system code model.

The testing, verification, and validation effort of the coupled code will be continuing. One potential study would be to verify the effects of different sets of data exchanged at the boundary interfaces, e.g. both the system and CFD codes could define one flow inlet and one pressure boundary. Another study could be performed to evaluate the error associated with the application of uniform boundary conditions in the CFD code. The CFD model could be extended to provide an estimation of the non-uniform distributions of the inlet velocity and temperature at the tank boundaries. Experimental measurements of the transient response of a liquid-metal reactor to an off-normal event are limited. One potential source of validation could be the IAEA benchmark problems associated with the EBR-II Shutdown Heat Removal Test-17 [16].

Along with the continuous development of physics modeling and component designs for the MOOSE-based SFR system analysis module, the coupled tool will be applied to the safety simulations of advanced sodium fast reactor designs. The target would be to develop a CFD model of the ABTR upper plenum, and couple this model to the existing system code model. A protected loss-of-flow transient would be performed that drives the system into the natural circulation regime. Thermal stratification would be expected in the upper plenum, and its influence on the system response will be evaluated with the coupled tool.

## References

1. M.E. Conner, E. Baglietto and A.M. Elmahdia, "CFD Methodology and Validation for Single-Phase Flow in PWR Fuel Assemblies," Nuclear Engineering and Design, 240, pp. 2088-2095 (2009).
2. W.D. Pointer, J.W. Thomas, T.H. Fanning, et al., "RANS-Based CFD Simulations of Sodium Fast Reactor Wire-Wrapped Pin Bundles," Proceedings of M&C 2009, Saratoga Springs, New York (2009).
3. D. Bestion, "From the Direct Numerical Simulation to System Codes – Perspective for the Multi-scale Analysis of LWR Thermalhydraulics," Nuclear Engineering and Technology, 242(6), pp.609-619 (2010).
4. T.H. Fanning, W.D. Pointer, and J.W. Thomas, "Multi-Resolution Modeling of Subassembly Pin Bundles for Advanced Fast Reactor Safety Simulations," Proceedings of M&C 2009, Saratoga Springs, New York (2009).
5. T. H. Fanning, ed., The SAS4A/SASSYS-1 Safety Analysis Code System, ANL/NE-12/4, Nuclear Engineering Division, Argonne National Laboratory, January 31, (2012).
6. T.H. Fanning and J.W. Thomas, "Integration of CFD into Systems Analysis Codes for Modeling Thermal Stratification during SFR Transients," Proceedings of NURETH-14, Toronto, Ontario, Canada, September 25-30, (2011).
7. S. Balay, J. Brown, K. Buschelman, V. Eijkhout, W. D. Gropp, D. Kaushik, M. G. Knepley, L. C. McInnes, B. F. Smith, and H. Zhang, PETSc Users Manual, ANL-95/11 – Revision 3.3, Argonne National Laboratory, (2012).
8. D. Gaston, C. Newman, G. Hansen, and D. Lebrun-Grandi'e, "MOOSE: A parallel computational framework for coupled systems of nonlinear equations," Nucl. Eng. Design, vol. 239, pp. 1768–1778, (2009).
9. D. Anders, R. Berry, D. Gaston, et al., "Demonstration of a Steady State Single Phase PWR Simulation with RELAP-7", INL/EXT-12-25924, May (2012).
10. R. Hu and T. H. Fanning, Argonne National Laboratory, unpublished information, August 31, (2012).
11. CD-adapco, "STAR-CCM+ 7.06 Manual," N.Y., (2012).
12. J.W. Thomas, T.H. Fanning, R. Vilim, L.L. Briggs, "Validation of the Integration of CFD and SAS4A/SASSYS-1: Analysis of the EBR-II Shutdown Heat Removal Test 17," Proceedings of ICAPP12, Chicao IL, June 24 – 28, (2012).
13. D.L. Aumiller, E.T. Tomlinson, W.L. Weaver, "An integrated RELAP5-3D and multiphase CFD code system utilizing a semi-implicit coupling technique," Nuclear Engineering and Design, 216, 77–87, (2002).
14. Davide Bertolotto, Annalisa Manera, Simon Frey, Horst-Michael Prasser, Rakesh Chawl, "Single-phase mixing studies by means of a directly coupled CFD/system-code tool," Annals of Nuclear Energy, 36, 310–316, (2009).
15. T. Sofu and J.W. Thomas, "Analysis of Thermal Stratification in the Upper Plenum of the Monju Reactor Vessel", NURETH-14, Toronto, Ontario, Canada, September 25-30, (2011).

16. T. Sumner and T.Y.C. Wei, Argonne National Laboratory, unpublished information, May 31, (2012).







**Nuclear Engineering Division**  
Argonne National Laboratory  
9700 South Cass Avenue, Bldg. #208  
Argonne, IL 60439

[www.anl.gov](http://www.anl.gov)



Argonne National Laboratory is a U.S. Department of Energy  
laboratory managed by UChicago Argonne, LLC